FRONTIERS OF PHYSICS

RESEARCH ARTICLE
Volume 18 / Issue 3 / 33304 / 2023

# Correlation-driven threefold topological phase transition in monolayer $OsBr_2$

San-Dong Guo[1,†], Yu-Ling Tao[1], Wen-Qi Mu[1], Bang-Gui Liu[2,3]

1 School of Electronic Engineering, Xi'an University of Posts and Telecommunications, Xi'an 710121, China
2 Beijing National Laboratory for Condensed Matter Physics, Institute of Physics, Chinese Academy of Sciences, Beijing 100190, China
3 School of Physical Sciences, University of Chinese Academy of Sciences, Beijing 100190, China
Corresponding author. E-mail: †sandongyuwang@163.com
Received July 22, 2022; accepted October 30, 2022



## ABSTRACT

Spin–orbit coupling (SOC) combined with electronic correlation can induce topological phase transition, producing novel electronic states. Here, we investigate the impact of SOC combined with correlation effects on physical properties of monolayer $OsBr_2$, based on first-principles calculations with generalized gradient approximation plus $U$ (GGA+$U$) approach. With intrinsic out-of-plane magnetic anisotropy, $OsBr_2$ undergoes threefold topological phase transition with increasing $U$, and valley-polarized quantum anomalous Hall insulator (VQAHI) to half-valley-metal (HVM) to ferrovalley insulator (FVI) to HVM to VQAHI to HVM to FVI transitions can be induced. These topological phase transitions are connected with sign-reversible Berry curvature and band inversion between $d_{xy}/d_{x^2-y^2}$ and $d_{z^2}$ orbitals. Due to $\bar{6}m2$ symmetry, piezoelectric polarization of $OsBr_2$ is confined along the in-plane armchair direction, and only one $d_{11}$ is independent. For a given material, the correlation strength should be fixed, and $OsBr_2$ may be a piezoelectric VQAHI (PVQAHI), piezoelectric HVM (PHVM) or piezoelectric FVI (PFVI). The valley polarization can be flipped by reversing the magnetization of Os atoms, and the ferrovalley (FV) and nontrivial topological properties will be suppressed by manipulating out-of-plane magnetization to in-plane one. In considered reasonable $U$ range, the estimated Curie temperatures all are higher than room temperature. Our findings provide a comprehensive understanding on possible electronic states of $OsBr_2$, and confirm that strong SOC combined with electronic correlation can induce multiple quantum phase transition.

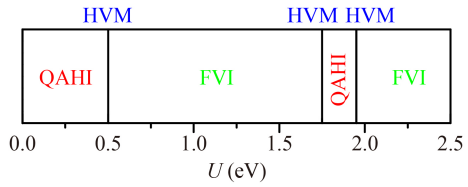

The intrinsic phase diagram of monolayer $OsBr_2$ with different $U$ values including quantum anomalous Hall insulator (QAHI), half-valley-metal (HVM) and ferrovalley insulator (FVI).

**Keywords** correlation, SOC, phase transition, piezoelectricity

## 1 Introduction

The effect of spin–orbit coupling (SOC) on physical properties of materials has attracted intensive attention. The SOC plays a key role for magnetocrystalline anisotropy, topological and valley physics [1–6]. For example, two-dimensional (2D) materials with long-range ferromagnetic (FM) order can be stabilized by SOC-induced magnetocrystalline anisotropy [1]. The SOC can also stabilize the topological phases by a nontrivial bandgap in quantum spin Hall insulator (QSHI) and quantum anomalous Hall insulator (QAHI) [2–4]. The SOC can induce spontaneous valley polarization in 2D magnetic semiconductors with special crystal symmetry, like 2H-$VSe_2$ [6].

The impact of electronic correlation on material properties has been a research hotspot [7–10]. Correlation-driven topological phases have been achieved in magic-angle twisted bilayer graphene [7]. Correlation-driven eightfold magnetic anisotropy can be realized in a 2D

Higher Education Press

https://doi.org/10.1007/s11467-022-1243-5

oxide monolayer [8]. Topological Fermi surface transition can be induced by varied electronic correlation in FeSe [9]. Coulomb interaction can induce quantum anomalous Hall (QAH) phase in (111) bilayer of $LaCoO_3$ [10]. Generally, the correlation effects are resultful in transition metal elements with localized $d$ electrons. For special crystal symmetry, electron correlation can dramatically enhance SOC effect of light elements in certain partially occupied orbital multiplets [11].

Recently, some novel electronic states, such as valley-polarized quantum anomalous Hall insulator (VQAHI) and half-valley-metal (HVM), have been predicted in many 2D materials [12–19]. For FeClF or $FeCl_2$ monolayer, increasing electron correlation can induce ferrovalley insulator (FVI) to HVM to VQAHI to HVM to FVI transitions with fixed out-of-plane magnetic anisotropy [12, 14]. However, with intrinsic magnetic anisotropy, no special VQAHI and HVM states exist in FeClF monolayer, which means that no topological phase transition is induced. For monolayer $RuBr_2$, with fixed out-of-plane magnetic anisotropy, the phase diagram is the same with that of FeClF monolayer [15]. The intrinsic phase diagram shows VQAHI and HVM states, but only one HVM state can exist. From FeClF to $RuBr_2$, these differences are because Ru atom has heavier atomic mass than Fe atom, which will lead to stronger SOC effects. The Os atom has more stronger SOC effects than Ru atom, which may give rise to other novelty effects. Recently, monolayer $OsBr_2$ with 1$H$-$MoS_2$ type structure is predicted to stable [20].

In this work, the electronic correlation effects on electronic structures of $OsBr_2$ monolayer are carefully investigated. Different from FeClF or $FeCl_2$ or $RuBr_2$, increasing electron correlation induces threefold topological phase transition in monolayer $OsBr_2$ with intrinsic out-of-plane magnetic anisotropy, which means that there are three HVM states and two VQAHI regions. Due to missed centrosymmetry, $OsBr_2$ is piezoelectric, and its piezoelectric properties are investigated. The combination of piezoelectricity, topology and/or ferrovalley (FV) in $OsBr_2$ monolayer provides a potential platform for multi-functional spintronic applications, and our works provide possibility to use the piezoelectric effect to control QAH or anomalous valley Hall effect.

## 2 Computational detail

The spin-polarized first-principles calculations are carried out within density-functional theory (DFT) [23, 24], as implemented in VASP code [25–27]. The projected augmented wave (PAW) method with generalized gradient approximation of Perdew–Burke–Ernzerhof (PBE-GGA) [28] exchange-correlation functional is adopted. The energy cut-off of 500 eV and total energy convergence criterion of $10^{-8}$ eV are used to attain accurate results. The force convergence criteria on each atom is set to be less than 0.0001 eV·Å$^{-1}$. A more than 18 Å cell height is used in the $z$ direction to prevent periodic images from interacting with each other. We use Γ-centered 24 × 24 × 1 k-mesh to sample the Brillouin zone (BZ) for structure optimization, electronic structures and elastic stiffness tensor, and 12 × 24 × 1 Monkhorst–Pack k-point mesh for FM/antiferromagnetic (AFM) energy and piezoelectric stress tensor with rectangle supercell. Within the rotationally invariant approach proposed by Dudarev et al, the GGA+$U$ method is employed to describe the correlated Os-$d$ electrons. The SOC effect is explicitly included, which is very key to investigate magnetic anisotropy energy (MAE), electronic and topological properties of $OsBr_2$ monolayer.

We use strain-stress relationship (SSR) and density functional perturbation theory (DFPT) method [29] to attain elastic stiffness tensor $C_{ij}$ and piezoelectric stress tensor $e_{ij}$. The 2D elastic/piezoelectric coefficients $C_{ij}^{2D}$/$e_{ij}^{2D}$ have been renormalized by $C_{ij}^{2D}/e_{ij}^{2D} = L_z C_{ij}^{3D}/e_{ij}^{3D}$, where the $L_z$ is the cell height along $z$ direction. The edge states are calculated with the maximal localized Wannier function tight-binding model by employing $d$-orbitals of Os atoms and $p$-orbitals of Br atoms [30, 31]. The Berry curvatures of $OsBr_2$ are attained directly from the calculated wave functions based on Fukui's method [32], as implemented in VASPBERRY code [33, 34]. For predicting Curie temperature ($T_C$) of $OsBr_2$, the 40×40 supercell and $10^7$ loops are used to achieve Monte Carlo (MC) simulations, as implemented in Mcsolver code [35].

## 3 Structure and magnetic properties

Similar to monolayer 1$H$-$MoS_2$, for monolayer $OsBr_2$, its Os atom layer is sandwiched by two Br atom layers through the Os-Br bonds, whose crystal structure is shown in Fig. 1, along with BZ with high-symmetry points in Fig. S1 of the Supplementary Information (SI). The $OsBr_2$ monolayer with $P\bar{6}m2$ symmetry (No.187) lacks centrosymmetry, indicating that it should possess piezoelectricity and FV properties. The symmetry of $OsBr_2$ is higher than that of FeClF with $P3m1$ symmetry (No. 156) due to broken vertical mirror symmetry [14]. These mean that only in-plane piezoelectric polarization exists in $OsBr_2$ monolayer, when it is subject to a uniaxial in-plane strain. When applying biaxial in-plane strain, the in-plane piezoelectric polarization will be suppressed. The lattice constants $a$ of $OsBr_2$ monolayer is optimized with varied $U$, as shown in Fig. S1 of the SI. The $a$ increases with increasing $U$, which can also be found in monolayer FeClF and $RuBr_2$ [14, 15]. And then, its magnetic, electronic and piezoelectric properties are investigated with varied $U$ by using the corresponding $a$.

Next, a rectangle supercell is used to explore the magnetic coupling of $OsBr_2$ monolayer, and three initial

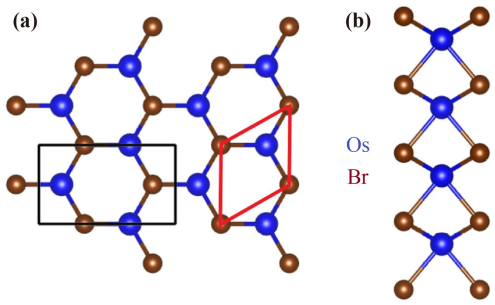


**Fig. 1** The top view **(a)** and side view **(b)** of crystal structure of $OsBr_2$ monolayer, and the rhombus primitive cell (rectangle supercell) is marked by the red (black) frame.

magnetic configurations of AFM1, AFM2 and FM ordering are considered. The AFM1 and AFM2 configurations are plotted in Fig. 1 of the SI. Their total energy difference $\Delta E$ between AFM1/AFM2 and FM ordering as a function of $U$ is plotted in Fig. 2. In considered $U$ range, $OsBr_2$ monolayer is a 2D intrinsic FM material. It is found that $\Delta E$ is sensitive to $U$, giving rise to important influence on $T_C$ of $OsBr_2$ monolayer. In view of the important role of magnetic anisotropy in realizing the long-range magnetic order and novel electronic states in 2D materials [13–15], the MAE of $OsBr_2$ monolayer is calculated from a difference in the obtained total energies with magnetization direction parallel or perpendicular to the plane of monolayer ($E_{MAE} = E_{(100)} - E_{(001)}$). Thus, the positive or negative MAE means that the easy magnetization axis is perpendicular or parallel to the plane of monolayer. The MAE vs. $U$ is plotted in Fig. 2, and the easy

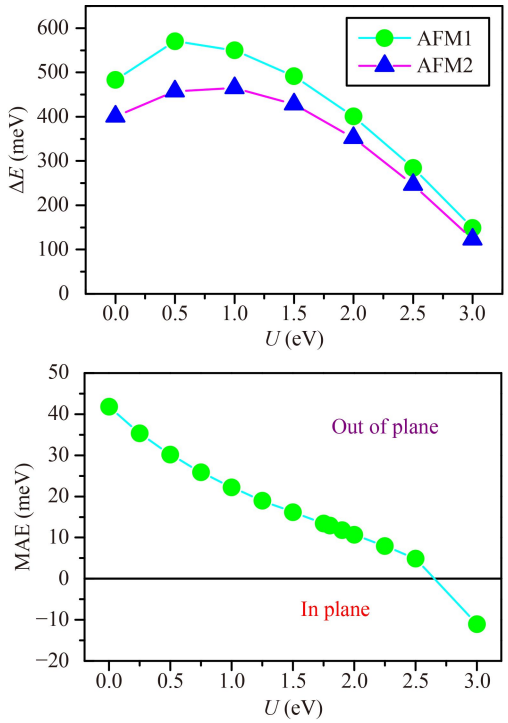


**Fig. 2** The energy differences $\Delta E$ between AFM1/AFM2 and FM ordering with rectangle supercell (see Fig. S1 of the SI) and MAE of $OsBr_2$ monolayer as a function of $U$.

magnetization axis changes from out-of-plane to in-plane one with critical $U$ value about 2.6 eV. Similar results can be found in monolayer FeClF and $RuBr_2$ [14, 15], but critical $U$ value of $OsBr_2$ is larger than their ones (1.45

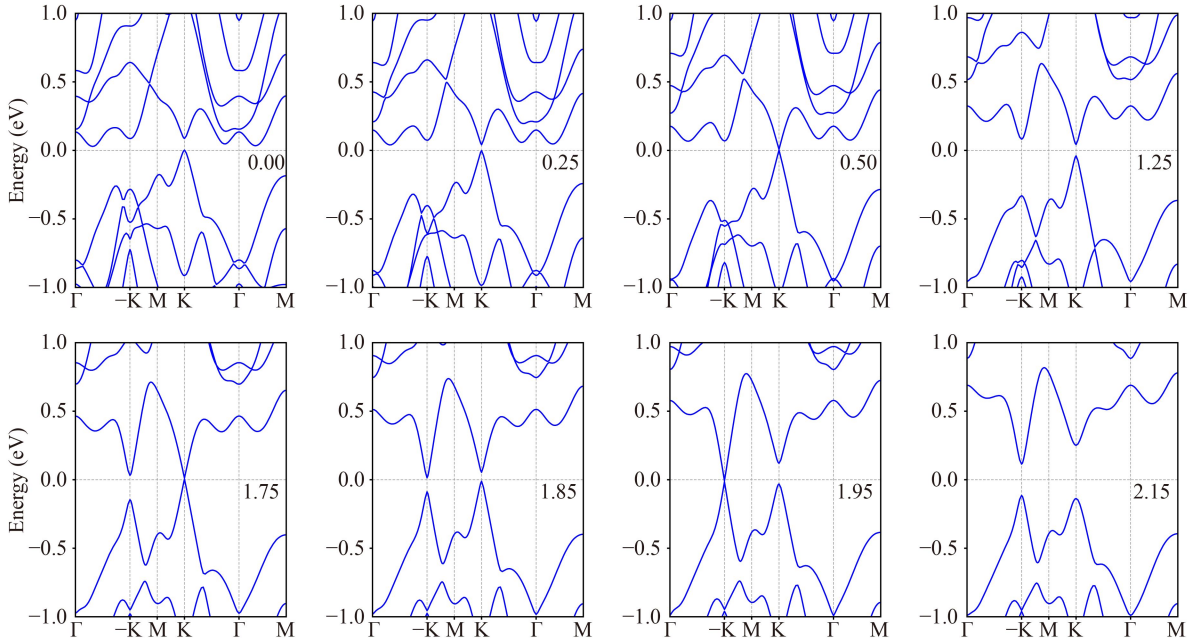


**Fig. 3** The energy band structures of $OsBr_2$ monolayer with out-of-plane magnetic anisotropy by using GGA+SOC at representative $U$ values.

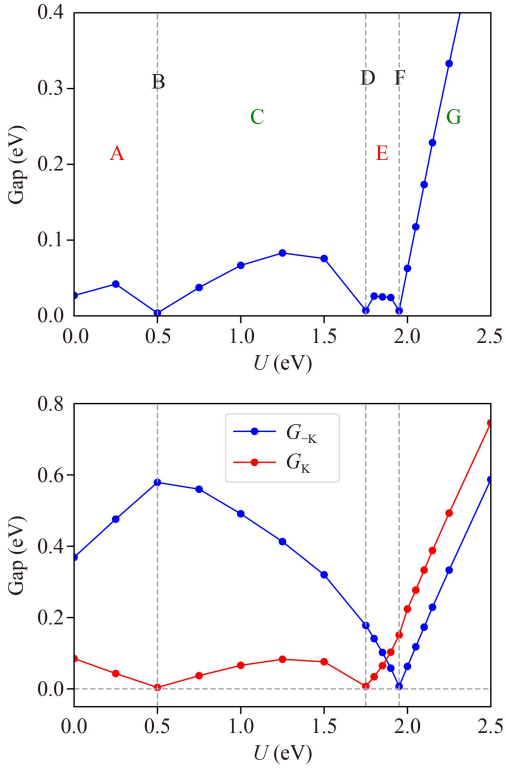


**Fig. 4** For $OsBr_2$ monolayer with out-of-plane magnetic anisotropy, the global energy band gap and energy band gaps for –K and K valleys as a function of $U$. A and E regions mean PVQAHI, and C and G regions mean PFVI, and B, D and F points mean PHVM.

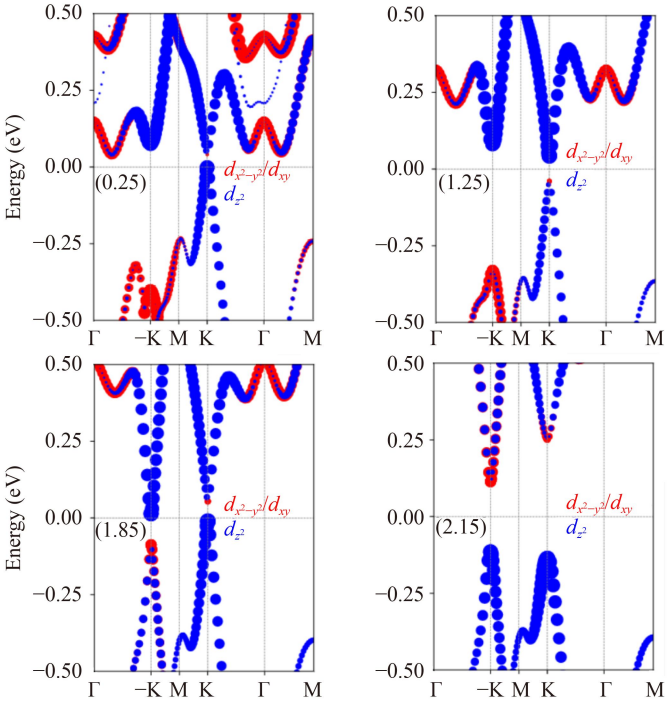


**Fig. 5** For $OsBr_2$ monolayer with out-of-plane magnetic anisotropy, the Os-$d_{x^2-y^2}/d_{xy}$ and $d_{z^2}$-orbital characters energy band structures at representative $U$ = 0.25 eV, 1.25 eV, 1.85 eV and 2.15 eV.

and 2.07 eV). The large critical $U$ value is very important to confirm intrinsic novel QAH and HVM states. It is well known that valence 5$d$ wave functions are more delocalized than those of 3$d$, and then 5$d$ transition-metals show very weak electron correlation. In previous works, the $U$ for Os-5$d$ electrons is taken as 0.5 eV for monolayer $OsO_2$ and 1.5 eV for the 5$d$-modified antimonene [21, 22]. At typical $U$ = 1.5 eV, the MAE of monolayer $OsBr_2$ is as high as 16.14 meV/Os, which means very stable out-of-plane magnetic anisotropy.

## 4 Topological phase transition

Electronic correlation combined with out-of-plane magnetic anisotropy can produce novel electronic states in some 2D materials [12–15], such as FV, QAH and HVM states. However, the in-plane magnetic anisotropy will lead to disappeared novel electronic states in these 2D materials [13–15]. Generally, Os-5$d$ electrons show very weak electron correlation [21, 22], and the easy magnetization axis of $OsBr_2$ monolayer is out-of-plane with $U$ being less than 2.6 eV. So, we only consider that the $U$ ranges from 0.00 eV to 2.50 eV, and the corresponding electronic properties are investigated. At some representative $U$ values, the energy band structures of $OsBr_2$ with GGA+SOC are shown in Fig. 3, and the evolutions of total energy band gap along with those at –K/K point as a function of $U$ are plotted in Fig. 4.

It is clearly seen that there are three points around $U$ = 0.5 eV, 1.75 eV and 1.95 eV, where the total energy band gap is closed. At these points, the HVM state can be achieved, whose conduction electrons are intrinsically 100% valley polarized [12]. However, these HVM states can be divided into two categories. At $U$ = 0.5 eV/1.75 eV, the band gap gets closed at K valley, while a band gap of 0.58 eV/0.18 eV is kept at –K valley. At $U$ = 1.95 eV, the band gap of –K valley is closed, while the band gap at K valley is 0.15 eV. The $U$ region can be divided into four parts by three HVM states.

As shown in Fig. 5, both valence and conduction valleys at –K and K points are primarily contributed by Os-$d_{x^2-y^2}/d_{xy}$ or $d_{z^2}$ orbitals in considered $U$ range. For 0.00 eV < $U$ < 0.50 eV, the $d_{x^2-y^2}$ and $d_{xy}$ orbitals dominate conduction band at K valley, while the valence band of K valley is mainly from $d_{z^2}$ orbitals (For example, $U$ = 0.25 eV). When $U$ is between 0.5 eV and 1.75 eV, the opposite situation can be observed with ones of 0.00 eV < $U$ < 0.50 eV (For example $U$ = 1.25 eV). For 1.75 eV < $U$ < 1.95 eV, the distribution of $d_{x^2-y^2}/d_{xy}$ and $d_{z^2}$ orbitals at K valley is opposite to one of 0.50 eV < $U$ < 1.75 eV (For example, $U$ = 1.85 eV). For the three regions, at –K valley, the $d_{z^2}$ orbitals dominate

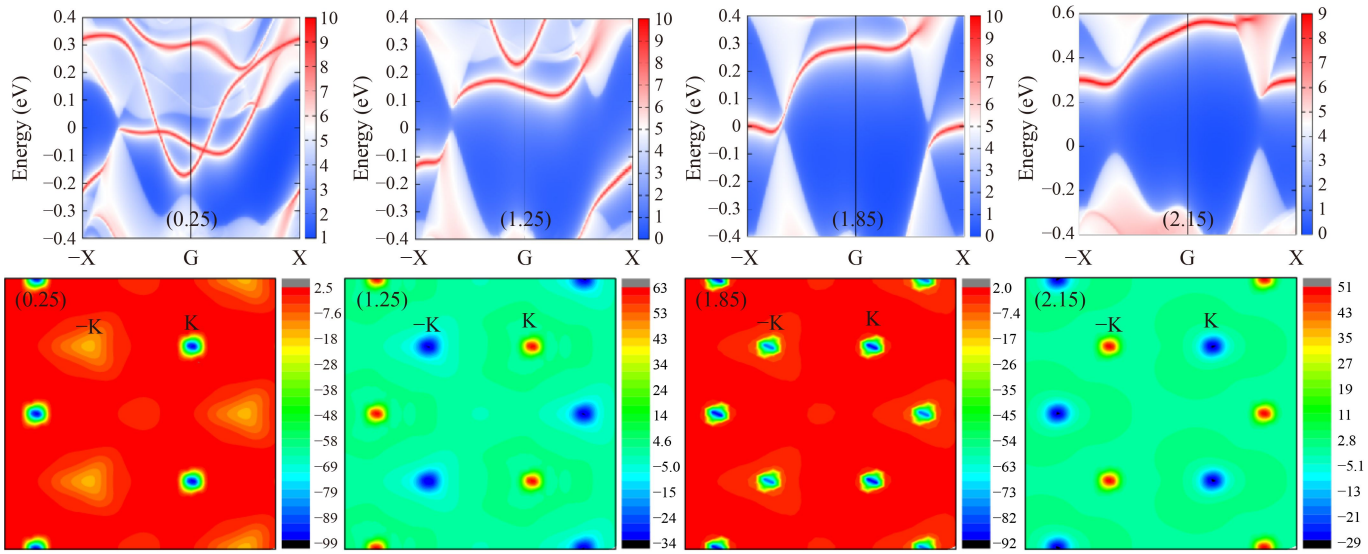


**Fig. 6** For $OsBr_2$ monolayer with out-of-plane magnetic anisotropy, the topological edge states (top) and Berry curvature distribution in 2D BZ (bottom) at representative $U = 0.25$ eV, 1.25 eV, 1.85 eV and 2.15 eV.

conduction band, while the valence band is mainly from $d_{x^2-y^2}/d_{xy}$ orbitals. These means that there are two-time band inversion between $d_{xy}/d_{x^2-y^2}$ and $d_{z^2}$ orbitals at K valley with increasing $U$. For the fourth region ($U >$ 1.95 eV), at –K valley, the distribution of $d_{x^2-y^2}/d_{xy}$ and $d_{z^2}$ orbitals is opposite to one of 1.75 eV $< U <$ 1.95 eV, but this is the same at K valley (For example, $U =$ 2.15 eV). This means another band inversion between $d_{xy}/d_{x^2-y^2}$ and $d_{z^2}$ orbitals at –K valley.

The three HVM states imply that the total gap of $OsBr_2$ monolayer closes and reopens three times. The special gap change along with band inversion suggest some topological phase transitions, and QAH state may exist in some regions. To confirm QAH phases, we calculate the edge states at representative $U = 0.25$ eV, 1.25 eV, 1.85 eV and 2.15 eV from four regions, which are plotted in Fig. 6. It is clearly seen that a nontrivial chiral edge state, connecting the conduction bands and valence bands, does exist in two regions (0.00 eV $< U <$ 0.50 eV and 1.75 eV $< U <$ 1.95 eV), implying a QAHI. The calculated Chern number is equal to minus one ($C = -1$), which is consistent with one obtained by integrating the Berry curvature within the first BZ. For the other two regions (0.50 eV $< U <$ 1.75 eV and $U >$ 1.95 eV), no nontrivial chiral edge state appears, suggesting a normal FM semiconductor. These mean that increasing $U$ can induce threefold topological phase transition in monolayer $OsBr_2$

These topological phase transitions are also connected with transformation of Berry curvature. At representative $U = 0.25$ eV, 1.25 eV, 1.85 eV and 2.15 eV, the distributions of Berry curvature are shown in Fig. 6, whose hot spots are around –K and K valleys. For two regions (0.50 eV $< U <$ 1.75 eV and $U >$ 1.95 eV), the opposite signs and different magnitudes around –K and K valleys can be observed. However, for the other two regions (0.00 eV $< U <$ 0.50 eV and 1.75 eV $< U <$ 1.95 eV), the Berry curvatures around –K and K valleys have the same signs and different magnitudes. With increasing $U$, triple topological phase transitions are produced, which are connected by three HVM states. In these transitions, the sign of Berry curvature at –K or K valley will flip. For example the first two topological phase transitions, the negative Berry curvature of K valley ($U = 0.25$ eV) changes into positive one ($U = 1.25$ eV), and then changes into negative one ($U = 1.85$ eV). The third topological phase transition leads to the sign flipping of Berry curvature at –K valley, and the negative Berry curvature ($U = 1.85$ eV) changes into positive one ($U =$ 2.15 eV). These suggest that sign-reversible Berry curvature can be induced by electronic correlation, which is related with topological phase transition.

## 5 Piezoelectric properties

Similar to monolayer $MoS_2$ [36], monolayer $OsBr_2$ lacks inversion symmetry, but possesses a reflection symmetry with respect to the central Os atomic plane. This means only in-plane polarization along the armchair direction is allowed when $OsBr_2$ is subject to a uniaxial in-plane strain. For biaxial in-plane strain, the in-plane piezoelectric polarization will be suppressed. The third-rank piezoelectric stress tensor $e_{ijk}$ and strain tensor $d_{ijk}$ are defined as

$$e_{ijk} = \frac{\partial P_i}{\partial \varepsilon_{jk}} = e_{ijk}^{elc} + e_{ijk}^{ion} \tag{1}$$

and

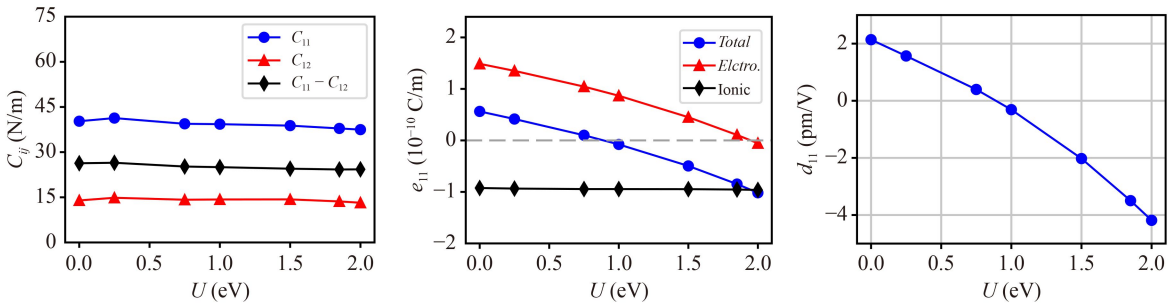


**Fig. 7** For $RuBr_2$ monolayer, the elastic constants $C_{ij}$, piezoelectric stress coefficient $e_{11}$ along with ionic and electronic parts, and piezoelectric strain coefficient $d_{11}$ as a function of $U$.

$$d_{ijk} = \frac{\partial P_i}{\partial \sigma_{jk}} = d_{ijk}^{elc} + d_{ijk}^{ion}, \tag{2}$$

in which $P_i$, $\varepsilon_{jk}$ and $\sigma_{jk}$ are polarization vector, strain and stress, respectively. The $e_{ijk}^{elc}/d_{ijk}^{elc}$ means clamped-ion piezoelectric coefficients with only considering electronic contributions. The $e_{ijk}/d_{ijk}$ means relax-ion piezoelectric coefficients as a realistic result, which is from the sum of ionic ($e_{ijk}^{ion}/d_{ijk}^{ion}$) and electronic ($e_{ijk}^{elc}/d_{ijk}^{elc}$) contributions. Analogous to monolayer $MoS_2$ [36], the piezoelectric stress and strain tensors of $OsBr_2$ by using Voigt notation can be reduced into:

$$\begin{pmatrix} e_{11} & -e_{11} & 0 \\ 0 & 0 & -e_{11} \\ 0 & 0 & 0 \end{pmatrix}, \tag{3}$$

$$\begin{pmatrix} d_{11} & -d_{11} & 0 \\ 0 & 0 & -2d_{11} \\ 0 & 0 & 0 \end{pmatrix}. \tag{4}$$

The only independent $d_{11}$ can be attained by $e_{ik} = d_{ij}C_{jk}$:

$$d_{11} = \frac{e_{11}}{C_{11} - C_{12}}. \tag{5}$$

First, we calculate elastic stiffness tensor $C_{ij}$ of $OsBr_2$ at some representative $U$ values, which are plotted in Fig. 7. For $OsBr_2$ monolayer, the Born criteria of mechanical stability [38] ($C_{11} > 0$ and $C_{11} - C_{12} > 0$) is satisfied for all $U$ values, indicating its mechanical stability. It is found that $C_{ij}$ have weak dependence on $U$. The $e_{11}$ of monolayer $OsBr_2$ is calculated with orthorhombic supercell by using DFPT method at some representative $U$ values. The piezoelectric stress coefficients $e_{11}$ (including ionic and electronic contributions) and piezoelectric strain coefficients $d_{11}$ are plotted in Fig. 7. When $U$ is less than about 1.85 eV, the electronic and ionic polarizations have opposite signs. For $U <$ 1.0 eV, the electronic contribution dominates the in-plane piezoelectricity. For 1.0 eV $< U <$ 1.85 eV, the ionic part dominates the $e_{11}$. According to Eq. (5), we calculate $d_{11}$ from previous calculated $C_{ij}$ and $e_{11}$. With increasing $U$, the $d_{11}$ changes from positive value to negative one, and the trend is the same with $e_{11}$. At representative $U$ = 1.5 eV, the absolute value of $d_{11}$ is 2.02 pm/V, which is close to one of $\alpha$-quartz ($d_{11}$ = 2.3 pm/V).

## 6 Electronic states

In considered $U$ range, $OsBr_2$ is an FV material, and the valley splitting for both valence and condition bands is plotted in Fig. 8. A possible way has been proposed to realize anomalous valley Hall effect in monolayer $GdCl_2$ by piezoelectric effect [37], not an external electric field. The $OsBr_2$ monolayer has the same structure with $GdCl_2$, and has FV and piezoelectric properties. So, $OsBr_2$ is also a piezoelectric FV (PFV) material, which can be used to realize piezoelectric anomalous valley Hall effect (PAVHE), as is illustrated in Fig. 2 of the SI. The in-plane longitudinal electric field $E$ is induced with an applied uniaxial in-plane strain by piezoelectric effect, and then anomalous valley Hall effect can be produced, The $U$ should be determined from future experiment result. If the $U$ falls into the two regions (0.00 eV $< U <$ 0.50 eV and 1.75 eV $< U <$ 1.95 eV), $OsBr_2$ monolayer will possess FV, QAH and piezoelectric properties, namely piezoelectric VQAHI (PVQAHI). For 0.00 eV $< U <$ 0.50 eV, chiral gapless edge mode mixes with trivial edge state in bulk gap, but the pure nontrivial chiral edge state can be observed for 1.75 eV $< U <$ 1.95 eV. In case of $U$ = 0.50 eV, 1.75 eV or 1.95 eV, $OsBr_2$ has HVM and piezoelectric properties, namely piezoelectric HVM (PHVM). These provide possibility to tune QAH and anomalous valley Hall effects by piezoelectric effect.

When reversing the magnetization orientation, the valley polarized state is also reversed. To explain this, the spin-polarized energy band structures of monolayer $OsBr_2$ are shown in Fig. 9 without SOC and with SOC for magnetic moment of Os along the positive and negative $z$ direction at representative $U$ = 1.25 eV. Without SOC, the bottom conduction band is from the spin-down channel, and there are a pair of energy extremes at –K and K points, yielding two inequivalent but degenerate valleys. However, the top valance band comes from the spin-up channel, and no energy extremes appear at –K

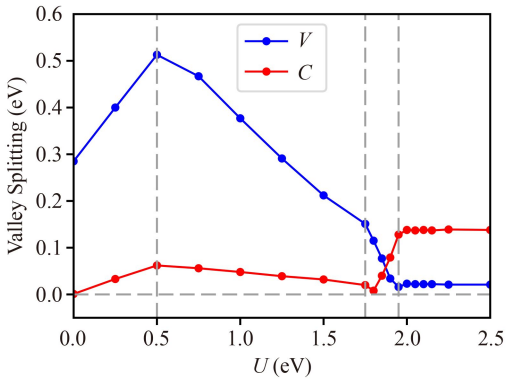


**Fig. 8** For out-of-plane magnetic anisotropy, the absolute value of valley splitting of monolayer $OsBr_2$ in both conduction ($C$) and valence ($V$) bands as a function of $U$.

and K points. In fact, these results depend on $U$ value. Increasing $U$ can lead to that both bottom conduction and top valance bands are from the spin-down channel, and have a pair of energy extremes at –K and K points, which are inequivalent but degenerate valleys (see Fig. 3 of the SI at $U = 2.15$ eV). When considering SOC, there are a pair of energy extremes at –K and K points for both conduction and valence bands, and the valley degeneracy is lifted (the –K/K valley state has a lower energy than K/–K valley for valence/conduction bands.), producing valley polarized state in $OsBr_2$. It is found that the valley polarization of valence bands is remarkably larger than one of conduction bands, which is because the –K and K valleys of valence bands are dominated by $d_{x^2-y^2}$ and $d_{xy}$ orbitals, while those of conduction bands are mainly from $d_{z^2}$ orbitals. Similar phenomenons can be found in many 2D FV materials [13–15, 39, 40]. As shown in Fig. 9(c), the valley polarization can be flipped by reversing the magnetization of Os atoms, namely, the K (–K) valley state has a lower energy than –K (K) valley for valence (conduction) bands. Manipulating direction of magnetization of $OsBr_2$ may be an efficient way to tune its valley properties.

The different magnetic orientation will affect the symmetry of $OsBr_2$, which has important influence on its electronic properties. For in-plane magnetic anisotropy, the FV and QAH properties will disappear. At representative $U = 1.85$ eV, with in-plane magnetic anisotropy, the energy band structures and topological edge states by using GGA+SOC are plotted in Fig. 10. It is clearly seen that the energies at –K and K points are degenerate for both valence and conduction bands, giving rise to no valley polarized state. The edge-state calculations show no chiral gapless edge modes within the bulk gap. So, the intrinsic out-of-plane magnetic anisotropy is very important to confirm these novel electronic states and topological transformations in considered $U$ range (0.00–2.50 eV).

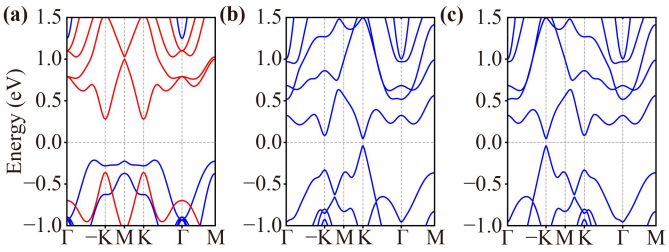


**Fig. 9** For out-of-plane magnetic anisotropy, the band structure of monolayer $OsBr_2$ **(a)** without SOC; **(b)** and **(c)** with SOC for magnetic moment of Os along the positive and negative $z$ direction, respectively. In (a), the blue (red) lines represent the band structure in the spin-up (spin-down) direction.

## 7 Curie temperature

As shown in Fig. 2, the electronic correlation effects ($U$) have important influence on the strength of FM interaction, which is related with $T_C$ of monolayer $OsBr_2$. The $T_C$ is estimated based on the Heisenberg model by MC simulations within Wolf algorithm. An effective classical spin Heisenberg model can be written as

$$H = -J\sum_{i,j} S_i \cdot S_j - A\sum_i (S_i^z)^2, \tag{6}$$

where $S_i/S_j$, $S_i^z$, $J$ and $A$ are the spin vectors of each Os atom, spin component parallel to the $z$ direction, the nearest neighbor exchange parameter and MAE, respectively. With rectangle supercell (see Fig. 1), the total energies of AFM1 ($E_{AFM}$) and FM ($E_{FM}$) ordering with normalized spin vector ($|S| = 1$) are given as

$$E_{FM} = E_0 - 6J - 2A, \tag{7}$$

$$E_{AFM} = E_0 + 2J - 2A, \tag{8}$$

where $E_0$ is the total energy of systems without magnetic coupling. The $J$ can be written as

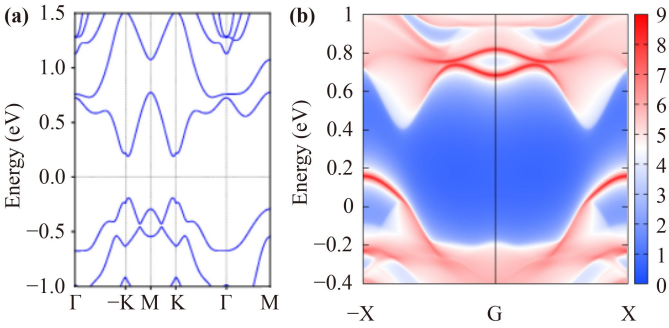


**Fig. 10** For $OsBr_2$ monolayer with in-plane magnetic anisotropy, the energy band structures **(a)** and topological edge states **(b)** at representative $U = 1.85$ eV.

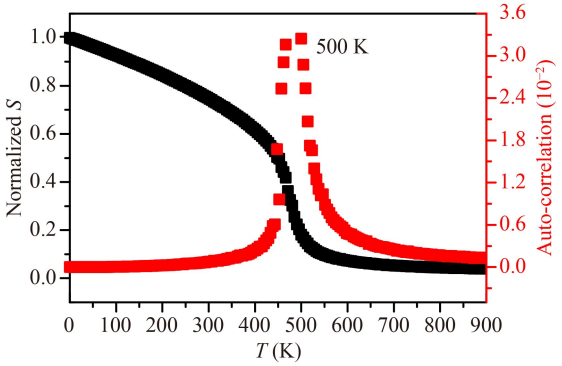


**Fig. 11** For monolayer $OsBr_2$, the normalized magnetic moment ($S$) and auto-correlation as a function of temperature with $U = 2.5$ eV.

$$J = \frac{E_{AFM} - E_{FM}}{8}. \quad (9)$$

According to Fig. 2, increasing $U$ weakens FM interaction, which will reduce $T_C$. We take $U = 2.50$ eV as a representative case, and the calculated normalized $J$ is 35.54 meV. The normalized magnetic moment and auto-correlation as a function of temperature are plotted in Fig. 11, and the predicted $T_C$ is about 500 K. In considered $U$ range (0.00–2.50 eV), the predicted $T_C$ is all higher than room temperature (see Fig. S4 of the SI). This implies that $OsBr_2$ is indeed a room-temperature ferromagnet.

## 8 Discussion and conclusion

Although Fe, Ru and Os atoms have same outer valence electrons, their SOC strengths are different due to different atomic mass. Increasing $U$ along with different SOC strength can induce different phase diagram of electronic state with fixed out-of-plane magnetic anisotropy. For monolayer $FeCl_2$ and $RuBr_2$, twofold topological phase transition with fixed out-of-plane magnetic anisotropy can be induced with increasing $U$ [12, 15], and the order is FVI to HVM to VQAHI to HVM to FVI. However, for $OsBr_2$, threefold topological phase transition can be observed, and it undergoes VQAHI, HVM, FVI, HVM, VQAHI, HVM, FVI, when $U$ increases. Strong SOC can lead to high critical $U$ value of out-of-plane to in-plane transition, which is very important to produce novel phase diagram. For example, for FeClF monolayer, the intrinsic phase diagram shows no special QAH and HVM states due to small critical $U$ (about 1.15 eV) [14]. However, intrinsic phase diagram of $OsBr_2$ shows both special QAH and HVM states with large critical $U$ of about 2.6 eV. The intrinsic phase diagrams for monolayer FeClF, $RuBr_2$ and $OsBr_2$ are plotted in Fig. 12. It is clearly seen that the intrinsic phase diagram of $OsBr_2$ is different from those of monolayer FeClF and $RuBr_2$.

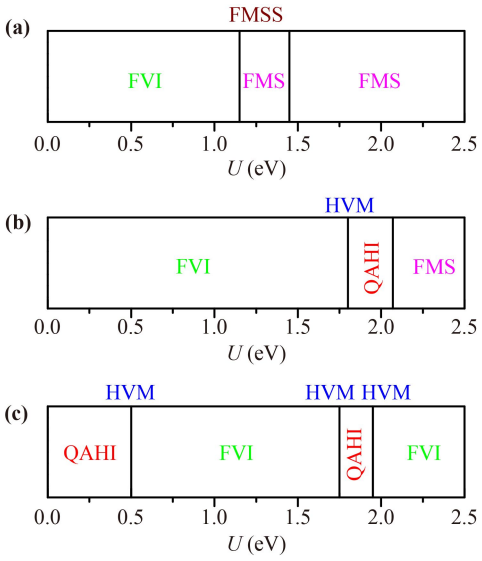


**Fig. 12** The intrinsic phase diagrams for monolayer FeClF **(a)**, $RuBr_2$ **(b)** and $OsBr_2$ **(c)** with different $U$ values including QAHI, HVM, FVI, FM semiconductor (FMS) and FM semimetal (FMSS).

The importance of electron correlations has been proved on the electronic state of monolayer $OsBr_2$. The different correlation strength (varied $U$) can give rise to different electronic state. For a given material, the correlation strength should be fixed, and $OsBr_2$ should belong to a particular electronic state in the phase diagram, which should be determined from related experiment. However, varied $U$ in producing novel electronic state is equivalent to applying different strain, which has been confirmed in $RuBr_2$ monolayer [15]. With fixed out-of-plane magnetic anisotropy for $RuBr_2$, the phase diagram with different $U$ values is similar with one with different strain. So, the rich electronic state and novel phase transitions can still be achieved in practice by strain. In fact, dual topological phase transition has been achieved in monolayer $OsBr_2$ by strain [20]. The sign-reversible valley-dependent Berry phase effects and QAH/HVM states in septuple atomic monolayer $VSi_2N_4$ has been achieved by strain [41].

In summary, we have demonstrated threefold topological phase transition with different $U$ in monolayer $OsBr_2$, which are related with sign-reversible Berry curvature and band inversions of $d_{xy}/d_{x^2-y^2}$ and $d_{z^2}$ orbitals at –K and K valleys. In considered $U$ range (0.00–2.50 eV), $OsBr_2$ is an intrinsic FVI with constant out-of-plane magnetic anisotropy. There are two QAH phase regions characterized by a chiral gapless edge mode, and the second region has pure non-trivial edge mode without mixture of characterless edge mode. The right boundary of the first QAH phase region and two boundaries of the second QAH phase region correspond to the HVM with fully valley polarized carriers. Due to lacking inversion symmetry, $OsBr_2$ is piezoelectric with only independent

$d_{11}$, which provides possibility to achieve anomalous valley Hall effect by piezoelectric effect. The estimated high $T_C$ confirm that these possible novel states can be realized in the high temperature. Our work deepens our understanding of strong SOC combined with correlation effects in monolayer $OsBr_2$, and provide a platform for multifunctional 2D material, such as PVQAHI and PFVI.

**Electronic supplementary material** Supplementary materials are available in the online version of this article at https://doi.org/10.1007/s11467-022-1243-5 and https://journal.hep.com.cn/fop/EN/10.1007/s11467-022-1243-5 and are accessible for authorized users.

**Acknowledgements** This work was supported by the Natural Science Basis Research Plan in Shaanxi Province of China (No. 2021JM-456), Graduate Innovation Fund Project in Xi'an University of Posts and Telecommunications (No. CXJJDL2021001), the National Natural Science Foundation of China (Grant No. 11974393) and the Strategic Priority Research Program of the Chinese Academy of Sciences (Grant No. XDB33020100). We are grateful to Shaanxi Supercomputing Center of China, and the calculations were performed on TianHe-2.

## References

1. B. Huang, G. Clark, E. Navarro-Moratalla, D. R. Klein, R. Cheng, K. L. Seyler, D. Zhong, E. Schmidgall, M. A. McGuire, D. H. Cobden, W. Yao, D. Xiao, P. Jarillo-Herrero, and X. Xu, Layer-dependent ferromagnetism in a van der Waals crystal down to the monolayer limit, *Nature* 546(7657), 270 (2017)
2. M. Z. Hasan and C. L. Kane, Topological insulators, *Rev. Mod. Phys.* 82(4), 3045 (2010)
3. X. L. Qi and S. C. Zhang, Topological insulators and superconductors, *Rev. Mod. Phys.* 83(4), 1057 (2011)
4. R. Yu, W. Zhang, H. J. Zhang, S. C. Zhang, X. Dai, and Z. Fang, Quantized anomalous Hall effect in magnetic topological insulators, *Science* 329(5987), 61 (2010)
5. X. Wan, A. M. Turner, A. Vishwanath, and S. Y. Savrasov, Topological semimetal and Fermi-arc surface states in the electronic structure of pyrochlore iridates, *Phys. Rev. B* 83(20), 205101 (2011)
6. W. Y. Tong, S. J. Gong, X. Wan, and C. G. Duan, Concepts of ferrovalley material and anomalous valley Hall effect, *Nat. Commun.* 7(1), 13612 (2016)
7. Y. Choi, H. Kim, Y. Peng, A. Thomson, C. Lewandowski, R. Polski, Y. Zhang, H. S. Arora, K. Watanabe, T. Taniguchi, J. Alicea, and S. Nadj-Perge, Correlation-driven topological phases in magic-angle twisted bilayer graphene, *Nature* 589(7843), 536 (2021)
8. Z. Cui, A. J. Grutter, H. Zhou, H. Cao, Y. Dong, D. A. Gilbert, J. Wang, Y. S. Liu, J. Ma, Z. Hu, J. Guo, J. Xia, B. J. Kirby, P. Shafer, E. Arenholz, H. Chen, X. Zhai, and Y. Lu, Correlation-driven eightfold magnetic anisotropy in a two-dimensional oxide monolayer, *Sci. Adv.* 6(15), eaay0114 (2020)
9. I. Leonov, S. L. Skornyakov, V. I. Anisimov, and D. Vollhardt, Correlation-driven topological Fermi surface transition in FeSe, *Phys. Rev. Lett.* 115(10), 106402 (2015)
10. Y. Wang, Z. Wang, Z. Fang, and X. Dai, Interaction-induced quantum anomalous Hall phase in (111) bilayer of $LaCoO_3$, *Phys. Rev. B Condens. Matter Mater. Phys.* 91(12), 125139 (2015)
11. J. Y. Li, Q. S. Yao, L. Wu, Z. X. Hu, B. Y. Gao, X. G. Wan, and Q. H. Liu, Designing light-element materials with large effective spin–orbit coupling, *Nat. Commun.* 13(1), 919 (2022)
12. H. Hu, W. Y. Tong, Y. H. Shen, X. Wan, and C. G. Duan, Concepts of the half-valley-metal and quantum anomalous valley Hall effect, *npj Comput. Mater.* 6, 129 (2020)
13. S. Li, Q. Q. Wang, C. M. Zhang, P. Guo, and S. A. Yang, Correlation-driven topological and valley states in monolayer $VSi_2P_4$, *Phys. Rev. B* 104(8), 085149 (2021)
14. S. D. Guo, J. X. Zhu, M. Y. Yin, and B. G. Liu, Substantial electronic correlation effects on the electronic properties in a Janus FeClF monolayer, *Phys. Rev. B* 105(10), 104416 (2022)
15. S. D. Guo, W. Q. Mu and B. G. Liu, Valley-polarized quantum anomalous Hall insulator in monolayer $RuBr_2$, *2D Mater.* 9, 035011 (2022)
16. J. Zhou, Q. Sun, and P. Jena, Valley-polarized quantum anomalous Hall effect in ferrimagnetic honeycomb lattices, *Phys. Rev. Lett.* 119(4), 046403 (2017)
17. T. Zhou, J. Y. Zhang, Y. Xue, B. Zhao, H. S. Zhang, H. Jiang, and Z. Q. Yang, Quantum spin–quantum anomalous Hall effect with tunable edge states in Sb monolayer-based heterostructures, *Phys. Rev. B* 94(23), 235449 (2016)
18. T. Zhou, S. Cheng, M. Schleenvoigt, P. Schüffelgen, H. Jiang, Z. Yang, and I. Žutić, Quantum spin-valley Hall kink states: From concept to materials design, *Phys. Rev. Lett.* 127(11), 116402 (2021)
19. S. D. Guo, W. Q. Mu, J. H. Wang, Y. X. Yang, B. Wang, and Y. S. Ang, Strain effects on the topological and valley properties of the Janus monolayer $VSiGeN_4$, *Phys. Rev. B* 106(6), 064416 (2022)
20. H. Huan, Y. Xue, B. Zhao, G. Y. Gao, H. R. Bao, and Z. Q. Yang, Strain-induced half-valley metals and topological phase transitions in $MBr_2$ monolayers (M = Ru, Os), *Phys. Rev. B* 104(16), 165427 (2021)
21. Y. J. Wang, F. F. Li, H. L. Zheng, X. F. Han, and Y. Yan, Large magnetic anisotropy and its strain modulation in two-dimensional intrinsic ferromagnetic monolayer $RuO_2$ and $OsO_2$, *Phys. Chem. Chem. Phys.* 20(44), 28162 (2018)
22. M. Zhang, H. M. Guo, J. Lv, and H. S. Wu, Electronic and magnetic properties of 5d transition metal substitution doping monolayer antimonene: Within GGA and GGA + $U$ framework, *Appl. Surf. Sci.* 508, 145197 (2020)
23. P. Hohenberg and W. Kohn, Inhomogeneous electron gas, *Phys. Rev.* 136(3B), B864 (1964)
24. W. Kohn and L. J. Sham, Self-consistent equations including exchange and correlation effects, *Phys. Rev.* 140(4A), A1133 (1965)

25. G. Kresse, *Ab initio* molecular dynamics for liquid metals, *J. Non-Cryst. Solids* 192–193, 222 (1995)
26. G. Kresse and J. Furthmüller, Efficiency of ab-initio total energy calculations for metals and semiconductors using a plane-wave basis set, *Comput. Mater. Sci.* 6(1), 15 (1996)
27. G. Kresse and D. Joubert, From ultrasoft pseudopotentials to the projector augmented-wave method, *Phys. Rev. B* 59(3), 1758 (1999)
28. J. P. Perdew, K. Burke, and M. Ernzerhof, Generalized gradient approximation made simple, *Phys. Rev. Lett.* 77(18), 3865 (1996)
29. X. Wu, D. Vanderbilt, and D. R. Hamann, Systematic treatment of displacements. strains .and electric fields in density-functional perturbation theory, *Phys. Rev. B* 72(3), 035105 (2005)
30. A. A. Mostofi, J. R. Yates, G. Pizzi, Y. S. Lee, I. Souza, D. Vanderbilt, and N. Marzari, An updated version of Wannier90: A tool for obtaining maximally-localized Wannier functions, *Comput. Phys. Commun.* 185(8), 2309 (2014)
31. Q. Wu, S. Zhang, H. F. Song, M. Troyer, and A. A. Soluyanov, WannierTools: An open-source software package for novel topological materials, *Comput. Phys. Commun.* 224, 405 (2018)
32. T. Fukui, Y. Hatsugai, and H. Suzuki, Chern numbers in discretized Brillouin zone: Efficient method of computing (spin) Hall conductances, *J. Phys. Soc. Jpn.* 74(6), 1674 (2005)
33. H. J. Kim, Webpage: github.com/Infant83/VASP-BERRY, 2018
34. H. J. Kim, C. Li, J. Feng, J.-H. Cho, and Z. Zhang, Competing magnetic orderings and tunable topological states in two-dimensional hexagonal organometallic lattices, *Phys. Rev. B* 93, 041404(R) (2016)
35. L. Liu, X. Ren, J. H. Xie, B. Cheng, W. K. Liu, T. Y. An, H. W. Qin, and J. F. Hu, Magnetic switches via electric field in BN nanoribbons, *Appl. Surf. Sci.* 480, 300 (2019)
36. K. N. Duerloo, M. T. Ong, and E. J. Reed, Intrinsic piezoelectricity in two-dimensional materials, *J. Phys. Chem. Lett.* 3(19), 2871 (2012)
37. S. D. Guo, J. X. Zhu, W. Q. Mu, and B. G. Liu, Possible way to achieve anomalous valley Hall effect by piezoelectric effect in a $GdCl_2$ monolayer, *Phys. Rev. B* 104(22), 224428 (2021)
38. E. Cadelano and L. Colombo, Effect of hydrogen coverage on the Young's modulus of graphene, *Phys. Rev. B* 85(24), 245434 (2012)
39. P. Zhao, Y. Dai, H. Wang, B. B. Huang, and Y. D. Ma, Intrinsic valley polarization and anomalous valley Hall effect in single-layer 2H-$FeCl_2$, *ChemPhysMater* 1(1), 56 (2022)
40. R. Li, J. W. Jiang, W. B. Mi, and H. L. Bai, Room temperature spontaneous valley polarization in two-dimensional FeClBr monolayer, *Nanoscale* 13(35), 14807 (2021)
41. X. Zhou, R. Zhang, Z. Zhang, W. Feng, Y. Mokrousov, and Y. Yao, Sign-reversible valley-dependent Berry phase effects in 2D valley-half-semiconductors, *npj Comput. Mater.* 7, 160 (2021)